Electronics and Electrical Engineering

AIMS Electronics and Electrical Engineering, 7(1): 100–120.
DOI: 10.3934/electreng.2023006
Received: 11 October 2022
Revised: 31 December 2022
Accepted: 06 January 2023
Published: 31 January 2023

http://www.aimspress.com/journal/ElectrEng

Research article

Miniature glass-metal coaxial waveguide reactors for microwave-assisted liquid heating

Gaurav Sharma[1] and Guennadi A. Kouzaev[2,*]

[1] Chemical Laboratory, Department of Electronic Systems, Norwegian University of Science and Technology (NTNU) (on leave), 7491 Trondheim, Norway
[2] Department of Electronic Systems, Norwegian University of Science and Technology (NTNU), 7491 Trondheim, Norway

*** Correspondence:** Email: guennadi.kouzaev@ntnu.no.

Abstract: Microwave (MW) irradiation is recognized as an effective tool in industries related to pharmaceuticals, chemistry, nanoparticle synthesis, food, etc. In the hardware field, some research efforts are concentrated on creating miniature reactors using low-cost technologies aimed at on-demand chemistry or parallel synthesis of many drugs.

This paper reports on the development and characterization of novel miniature chemical-resistant glass-metal coaxial reactors based on a modified Liebig condenser. It is composed of two concentric glass tubes, one for the central conductor carrying MW current, and the other for the copper-foiled cylinder surrounding the first pipe. The gap between them is filled with a liquid that is pumped and evacuated by using shielded thin inlet/outlet glass tubes, which are melted and opened into this cylindrical cavity. The reactor's geometry allows for the direct soldering of miniature MW SMA coaxial connectors of 50-Ω impedance.

The developed components are studied analytically, numerically and experimentally. The frequency properties of reactors are measured with a network analyzer. The temperature trends are explored by using a variable high-power MW generator, power meters and temperature sensors.

These reactors demonstrate their relative insensitivity toward variations in the permittivity of filling liquids in the range of $3.75 < \varepsilon < 30$, as shown in simulations and measurements. They demonstrate the increase by two orders in the longitudinal modal penetration depth and a more homogeneous heating along reactors as compared to their hollow coaxial prototypes.

These glass-metal miniature reactors can be used in on-demand continuous-flow accelerated liquid heating, chemistry and pharmacy.

Keywords: coaxial waveguide reactor; microwave-assisted heating; microwave-assisted chemistry; chemistry-on-demand

1. Introduction

Microwave (MW)-assisted chemistry and food processing show their effectiveness for the ages of their use in domestic, laboratory and industrial areas [1,2]. This chemistry is attractive because of the reactors' volume-distributed electromagnetic (EM) heating field.

Conventionally, large ovens are used for the reagents dissolved in polar and/or conducting solutions [1–3]. Different reactors on rectangular, cylindrical [1–9], coaxial [10–19] and microstrip-based waveguides [13,20–23] have been published for batch and continuous-flow chemistry. The main modes of the last two waveguides have no cut-off frequencies, being transversal EM (TEM) ones, and these reactors can be tailored to any size at the industrial MW frequency. Unfortunately, the extension of their volumes is limited by the short penetration depth of the EM waves in lossy liquids.

For instance, in Ref. [12], the cross-sectional scalability of coaxial reactors is proposed by adding many inner conductors to provide a more homogeneous EM field distribution. See Ref. [19], where it is confirmed in numerical simulations.

The miniature reactors on the TEM modes are attractive in on-demand chemistry, as they allow exact amounts of chemicals to be synthesized [24–26]. Developing these reactors requires a multi-physical approach, numerical software tools and analytical estimates. Theoretical simulations of heating liquids by MWs are associated with many difficulties. The first is that the exact models of fluids at different temperatures and pressure conditions are unknown. Most of the published formulas have been derived from measurements. These data, in turn, have some instrumental and other limits of accuracy. For instance, the experimental results are method-dependent [27], and the discrepancy between the measurements of different techniques can even reach 17%.

In Ref. [13], the approximate models of water, methanol and ethanol were created by using some published results, and these models will be used in our contribution. The miniature coaxial- and strip-based reactors considered in [13,15,16] are for static and continuous-flow MW heating. A universal setup was used for these experimentations with strip heaters [13] and a shielded coaxial waveguide [16] (Figure 1). In these cited papers, an analytical theory is developed to describe the EM, thermal and liquid motion phenomena.

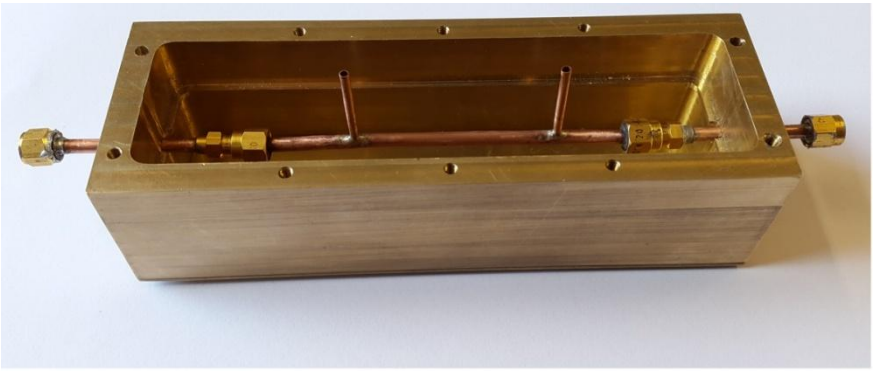

Figure 1. Miniature coaxial waveguide reactor [15].

Our theoretical and experimental results with the hollow coaxial reactors show fast heating of high-loss liquids only in a relatively small area near the input of MW power. In a continuous-flow regime, it means a smaller residence time of fluids in the strong EM field. Then, a more extended distribution of the heating field occurs only with low-loss liquids.

In addition, the characteristic impedance of these hollow coaxial reactors and their electrical length are highly dependent on the filling liquids. Then, each mixture may require a specific high-power-rated matching device.

This research aims to develop and characterize novel reactors with an extended modal penetration depth of MWs along these reactors that are tolerant of variations of the temperature-dependent dielectric permittivity and chemical activity of the heated fluids. It is reached by using multi-layered glass-metal waveguides whose geometry and dielectric filling were chosen to satisfy these requirements.

2. Novel glass-metal coaxial reactor

A new design is proposed to reduce the mentioned limitations of hollow coaxial reactors. It is based on a miniaturized Liebig condenser [28] (re-developed by us) that has been adapted to MW-assisted heating (Figure 2).

2.1. Geometry of the proposed reactor

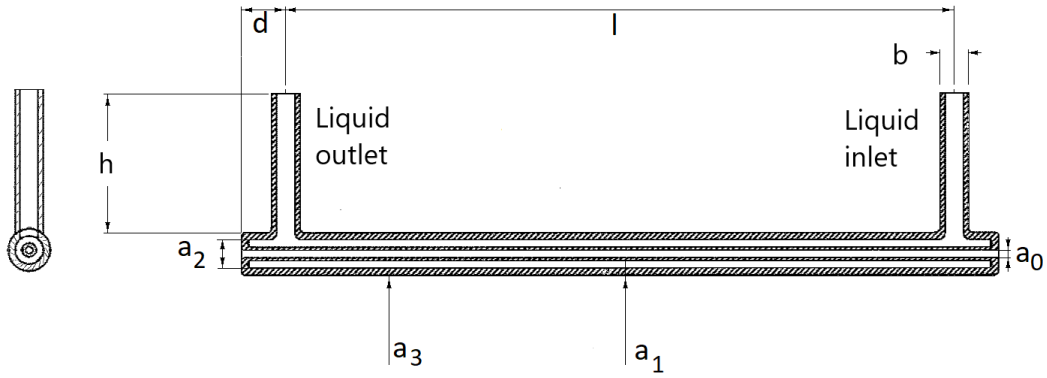

Figure 2. Draft of a miniature Liebig glass condenser.

The classical Liebig design consists of an inner tube (with an outer diameter (OD) a_1 and inner diameter (ID) a_0) filled with a hot liquid and an outer pipe $\left(\text{OD/ID} = a_3 / a_2\right)$ with a cold cooling fluid flowing in the gap between these pipes.

In our reactors [18], the inner tube $\left(\text{OD/ID} = a_1 / a_0\right)$ serves as the cavity for the central conductor (Figure 3). The outer pipe is shielded by copper foil (Figure 4). Altogether, they form a layered coaxial waveguide, and a lossy liquid moving in the gap between these tubes is heated by the conductor's EM field. Thus, the central wire is separated from the fluid under heating that may be corrosive to metals. Besides, the design prevents the electric discharge effect through conducting liquids.

The geometry of the glass body has been adapted to the 50-Ω RG401 coaxial cable environment [29]. Besides, the narrow channel between the central tube and the outer one (Figure 2) prevents the essential radial fluid convection, leading to the unpredictability of the yield of chemical reactions [14].

Figure 3. Reactor's glass body with an embedded silver-plated wire.

2.2. Reactor's materials, manufacturing techniques and a measurement test fixture

The quartz and borosilicate glass bodies of the miniature Liebig condensers were manufactured according to our drafts in *Andrews Glass Co*. (Appendix, Table 1, row 1) and *Sandfire Scientific, Ltd*. (Appendix, Table 1, rows 2 and 3).

A simple technique that is pertinent for manufacturing research reactor samples is proposed. We covered the outer tube $\left(\mathrm{OD/ID} = a_3 / a_2\right)$ with an adhesive copper foil of 0.05-mm thickness (Appendix, Table 1, row 4). This foil has a shielding effectiveness of 53–33 dB for frequencies of 1–10 GHz, which is high enough to avoid noticeable EM parasitic leakage [30,31]. Additionally, this shielding can be manufactured by applying vacuum and electroplating depositions of thermally-matched metals to the reactor's body to achieve improved adhesion of this layer to glass material, making this design usable in chemical and pharmaceutical industries. In this case, the reactor can be covered by a protective coat to prevent the corrosion of the metal shield in the case of occasional leakage.

The MW coaxial connectors (Appendix, Table 1, row 5) were soldered to this shield by using a conducting paste (Appendix, Table 1, row 6) and a hot-air soldering iron.

An example of these completed reactors mounted on a universal measurement board is shown in Figure 4. This setup allows for the measurement of items of various lengths. The SMA female-to-female right angles will prevent repeated rotational stress on soldered connectors with each joining of coaxial cables.

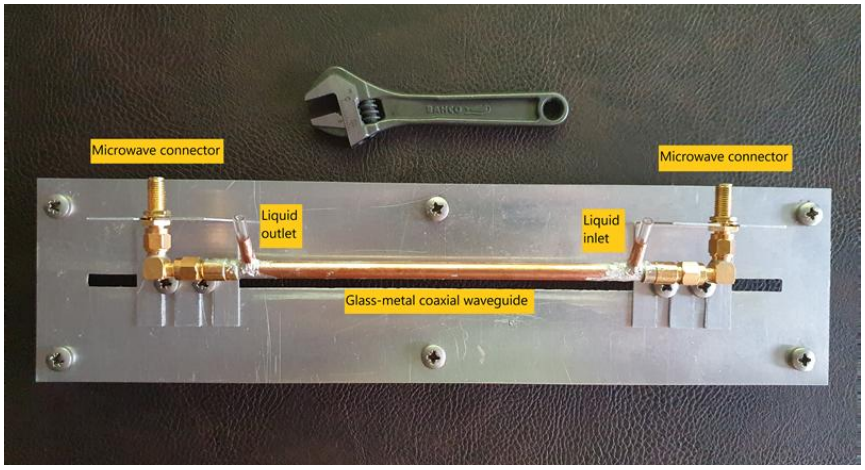

Figure 4. Glass-metal coaxial reactor in a measurement test fixture.

3. Theory and simulation results for glass-metal coaxial waveguides

3.1. Quasi-TEM analytical theory

The main element of the designed reactors is a regular glass-metal coaxial waveguide partially filled with liquid. This waveguide can be simulated analytically, matching the fields on the boundaries of layers. The longitudinal propagation constants of the modes were derived by solving transcendental dispersion equations, as is common in electromagnetism [32]. Numerical software tools are helpful as well in simulations.

For practical calculations, approximate analytical expressions can be obtained, supposing the quasi-TEM nature of the main mode of multi-dielectric coaxial waveguide [33,34]. In this case, the layered dielectric is substituted by an equivalent homogeneous one with the permittivity ε_{eq} known from the theory of multi-layered capacitors and antennas [35]:

$$\frac{1}{\varepsilon_{\text{eq}}} = \sum_{i=1}^{3} \frac{1}{\varepsilon_i} \frac{h_i}{h} \tag{1}$$

where ε_i is the relative dielectric permittivity of the *i*-th layer, $h_i = a_i - a_{i-1}$ (see Figure 5a) is the *i*-th layer's thickness and $h = \sum_{i=1}^{3} h_i$. Then, the longitudinal propagation constant $k_z = k_0\sqrt{\varepsilon_{\text{eq}}}$, where $k_0 = \omega/c$, with ω as the driving cycling frequency and c stands for the light velocity. If the dielectric filling is lossy, then $k_z = k_z' - jk_z''$ with j as the imaginary unit.

The conductor loss constant α_c, in the first approximation, can be calculated independently of the dielectric loss [36]:

$$\alpha_c = \frac{\text{Re}(Z_s)}{W_{\text{TEM}}} \frac{r_0 + r_3}{2r_0 r_3 \log(r_3/r_0)}, \tag{2}$$

where $Z_s = (1+j)\frac{1}{\sigma\Delta_0}$, $\Delta_0 = \sqrt{\frac{2}{\omega\mu_0\mu\sigma}}$, μ_0 is the absolute vacuum permeability, μ is the relative permeability of the coaxial conductors, and σ is their specific conductivity. In (2), $W_{\text{TEM}} = 120\pi\sqrt{\frac{1}{\text{Re}(\varepsilon_{\text{eq}})}}$, and $r_{0,3}$ are the radii of the inner and outer conductors correspondingly. Then, the longitudinal propagation constant is $k_z = k_z' - j(k_z'' + \alpha_c)$.

Another parameter needed for further treatment of this quasi-TEM mode is the characteristic impedance Z_c [37]:

$$Z_c = \frac{138}{\sqrt{\varepsilon_{\text{eq}}}} \lg\left(\frac{a_3}{a_0}\right). \tag{3}$$

3.2. Results of numerical and analytical simulations of regular glass-metal coaxial waveguides

The proposed reactor's layered design allows liquid placement in the area with a relatively smooth radial distribution of the EM field of a moderate intensity by varying the thickness of the

walls of tubes, similar to Ref. [14]. It can increase the modal longitudinal penetration depth and liquid residence time in the MW high-level heating field.

Significant work has been performed to confirm our preliminary ideas through the use of numerical simulation (COMSOL software tool [38]), analytical simulation (Eqs (1)–(3)) and optimization of the initial geometry of the reactors.

For comparison, Figure 5 shows the electric fields of layered (a) and conventional (b) coaxial waveguides, as calculated by using the COMSOL software tool. It is seen that liquid layer 2 is in an area with a moderately intense electric field (Figure 5a) that increases the modal longitudinal penetration depth $l_p = -1/\mathrm{Im}(k_z)$ in a couple of orders relave to the coaxial waveguide wholly filled by a lossy liquid (Figure 5b).

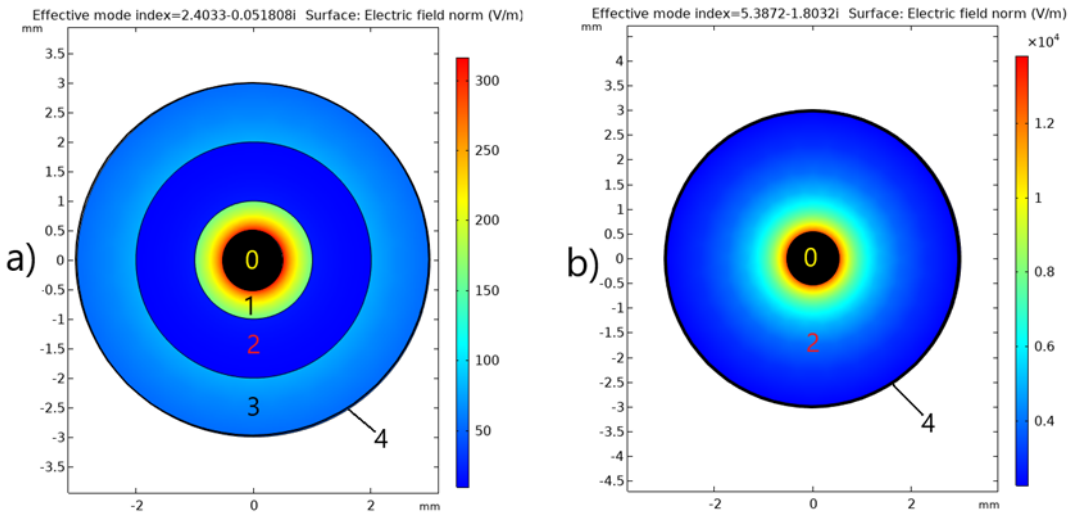

Figure 5. Electric field intensity distributions along the cross sections of a) glass-metal multi-layered and b) uniformly filled coaxial waveguides.

Conductors marked by 0 and 4 are ideal. Glass material (layers 1, 3) is fused quartz with a relative dielectric permittivity $\varepsilon_{\mathrm{quartz}} = \varepsilon' - j\varepsilon'' = 3.75 - j0.0004$ [39]. Layer 2 in Figure 5a is filled with methanol $(\mathrm{CH_3OH})$ with a relative dielectric permittivity $\varepsilon_{\mathrm{MT}} = 25.77 - j16.66$ [13] at a frequency $f = 2.45$ GHz . The diameters of the concentric layers were $a_0 = 1$ mm , $a_1 = 2$ mm , $a_2 = 4$ mm and $a_3 = 6$ mm . The coaxial waveguide in Figure 5b, which had central and outer conductor diameters of $a_0 = 1$ mm and $a_3 = 6$ mm, respectively, was filled with methanol. The field maps were computed by using the COMSOL Multiphysics software tool [38] with an extremely fine mesh. The effective mode index here is the normalized propagation constant k_Z/k_0 .

Our analytical results have been compared with the COMSOL Multiphysics simulations. The data are shown in Figure 6, where the curves were calculated by using Eq (1), and the markers are for COMSOL's results.

Simulations were performed for the air-, methanol- and ethanol-filled quartz-metal coaxial waveguides in the frequency and temperature domains. The complex permittivity values for methanol and ethanol were calculated by using formulas from Ref. [13].

The most significant difference between the analytical and COMSOL software simulations is seen for the waveguide (Figure 5a) filled with ethanol. At frequencies of 1–3 GHz, the average deviation of $\mathrm{Re}(k_z/k_0)$ was 0.9–2.75%.

Our model was obtained by supposing a TEM mode propagating along these transmission lines, meanwhile, according to Refs. [33,34], this main mode at low frequencies is a hybrid one with small longitudinal components of the electric and magnetic fields. With the frequency, this wave is transformed to a TM_0 mode with a stronger longitudinal electric field. It increases the difference between the full-wave and analytical calculations, as can be seen in Figure 6. In general, the layered design of lossy transmission lines somewhat complicates the dependence of the propagation constants on the waveguide filling [33,34,40,41].

Thus, with relatively good accuracy, the simple quasi-TEM formula (Eq (1)) can be used to design the glass-metal coaxial waveguides. Another important conclusion is that, despite the difference in permittivity between methanol and ethanol, the real parts of the propagation constants of a glass-metal coaxial waveguide filled with these fluids stay close to each other. Besides, they are weakly dependent on frequency (Figure 6a) and temperature (Figure 6b).

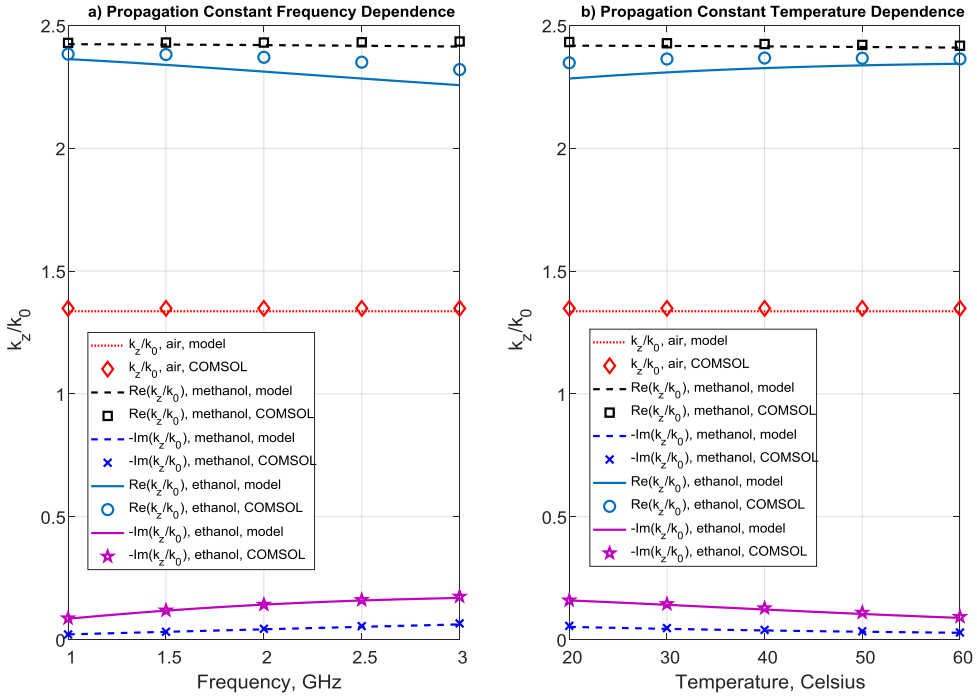

Figure 6. Characterization of regular quartz-metal coaxial waveguide filled by air, methanol or ethanol. (a) Frequency dependences of the normalized modal propagation constant k_z/k_0, as calculated analytically and numerically at the temperature $t = 21^{\circ}\mathrm{C}$. (b) Temperature dependences of the normalized modal longitudinal propagation constant k_z/k_0, as calculated analytically and numerically at the frequency $f = 2.45$ GHz. The relative permittivity of liquids is according to [13]. The material of the central conductor and outer shield is ideal. The wire diameter $a_0 = 1$ mm. The diameters of the quartz tubes were as follows: $a_0 = 1$ mm, $a_1 = 2$ mm, $a_2 = 4$ mm and $a_3 = 6$ mm.

Another outcome of the layered design is the essential decrease (in two orders) of the loss constants relative to a wholly filled coaxial waveguide of the same geometry [16]. It increases the

modal longitudinal penetration depth $l_p = -1/\mathrm{Im}(k_z)$ and smooths the heating field distribution along these waveguides.

Figure 7 shows the complex impedance behavior versus frequency (a) and temperature (b) for the air-, methanol- and ethanol-filled waveguides. It is seen that methanol and ethanol filling allows for a decrease of the characteristic impedance down to 45–47 Ω from 80 Ω for an air-filled coaxial waveguide of the same geometry. Additionally, the waveguides filled with ethylene glycol [42] $\left(f = 1-3\ \mathrm{GHz},\ t = 25^{\circ}\mathrm{C},\ 55^{\circ}\mathrm{C}\right)$ and 1,2- propanols [43] $\left(f = 2.45\ \mathrm{GHz},\ t = 21^{\circ}\mathrm{C}\right)$ have been modeled, and they also provide the 50-Ω-range characteristic impedance.

Further modeling shows that this impedance order (45–55 Ω) is for all liquids with a relative dielectric permittivity within the range of $3.75 < \varepsilon' < 30$ due to the chosen waveguide geometry being close to that of PTFE (Polytetrafluoreten)-filled RG401 coaxial waveguide [29] and the use of layered quartz. It gives a reflection coefficient of no more than -12 dB for a 50-Ω load, which is low enough in MW energy. The known substantial frequency and temperature variations of the liquid permittivities in the mentioned range change the characteristic impedance only for a few ohms, leaving this parameter close to 50 Ω, as seen in Figure 7. Then, it allows for the connection of a generator directly to the reactors without additional temperature-following matching circuits, which are very bulky at high MW powers. Further minimization of the reflection can be realized by tuning the length of the reactors and the positions of the inlets/outlets (Figure 2).

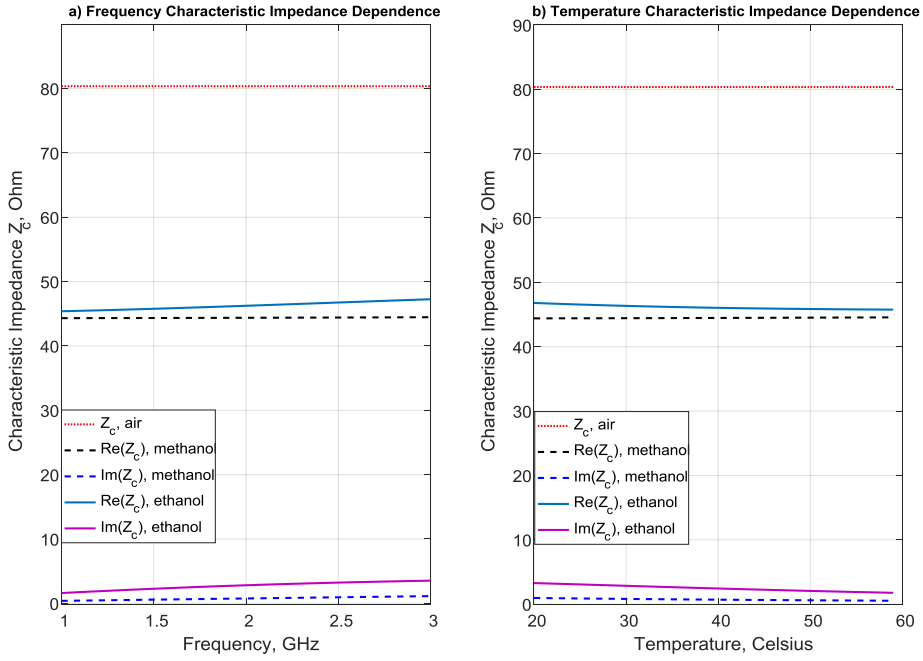

Figure 7. Characterization of regular quartz-metal coaxial waveguides filled by air, methanol or ethanol. (a) Frequency trends of the characteristic impedance Z_c calculated at the temperature $t = 21^{\circ}\mathrm{C}$. (b) Temperature trends of the characteristic impedance Z_c calculated at the frequency $f = 2.45$ GHz. The relative dielectric permittivity of liquids is according to [13]. The material of the central conductor and outer shield is ideal. The wire diameter $a_0 = 1$ mm. The diameters of the quartz tubes were as follows: $a_0 = 1$ mm, $a_1 = 2$ mm, $a_2 = 4$ mm and $a_3 = 6$ mm.

4. Measurement setups

4.1. Measurements of scattering characteristics of reactors

Measurements of the S-matrices of experimental samples at room temperature were performed by using the reactor test fixture shown in Figure 4. A handheld network analyzer (Appendix, Table 1, row 8) was used to obtain these data. For this purpose, this instrument was preliminarily calibrated. The measurement data of a reactor with the connectors (Figure 4) were written in the Touchstone format and visualized using a Matlab code.

4.2. Experimental setup for MW heating study

A block diagram of an experimental setup for the study of liquid heating in the designed reactors is shown in Figure 8. It consisted of a 2.45-GHz GaN generator of variable power $P = 0 - 250$ W (see Appendix, Table 1, row 14) and a reflectometer (Appendix, Table 12, row 15). This generator was connected directly to the reactor's test fixture (Reactor board) through the mentioned reflectometer. It allowed us to measure the generator and reflected powers by using the MW meters $\mathrm{PM}_{1,2}$ (Appendix, Table 1, rows 16 and 17).

Excess of the non-absorbed power in the reactor was transferred to a high-power 50-Ω load L (Appendix, Table 1, row 18) and absorbed there. A small portion of it was transferred to a power meter PM_3 (Appendix, Table 1, row 20) by a 20-dB directional coupler DC (Appendix, Table 1, row 19).

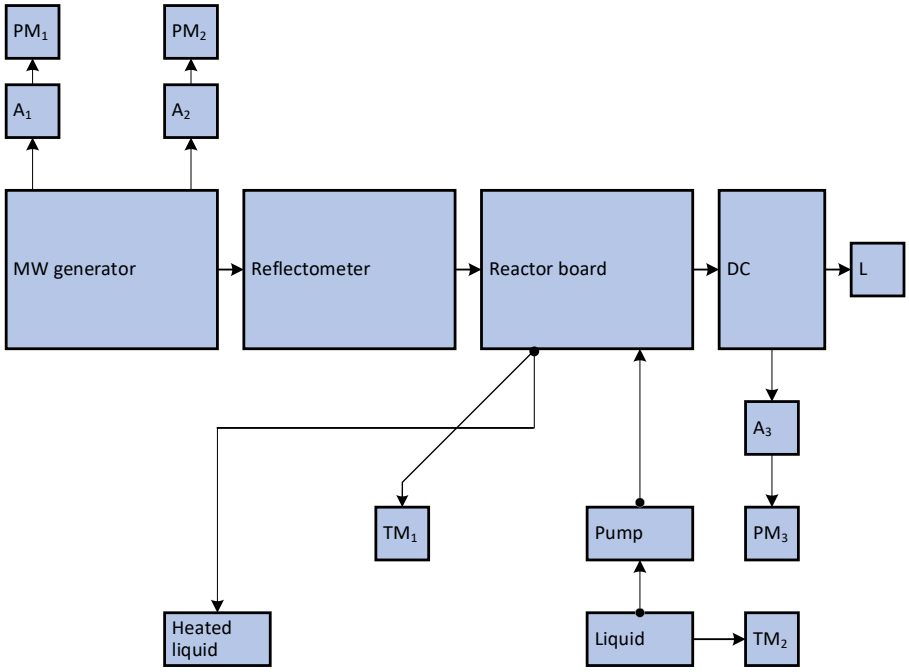

Figure 8. Block diagram of a setup for the MW-assisted heating of liquids in coaxial reactors; PM_{1-3}: MW power meters, $\mathrm{A}_{1\text{-}3}$: attenuators, DC: directional coupler, L: load (R_L = 50 Ω) and $\mathrm{TM}_{1,2}$: thermometers.

Attenuators $A_{1\text{-}3}$ (Appendix, Table 1, rows 21, 22 and 23) were included to adjust the power levels to the values acceptable by these meters. All MW components were connected directly or through coaxial cables (Appendix, Table 1, row 24); see Figure 9.

A liquid of a pre-measured temperature (sensor TM_2, Appendix, Table 1, row 25) was moved by a peristaltic pump (Appendix, Table 1, row 26) to the reactor. This fluid passed this reactor, and it was directed to a vessel for heated fluid. Inside the reactor, the temperature of this fluid was measured directly by using an optic fiber thermometer TM_1 (Appendix, Table 1, row 27) that is invulnerable to intense EM irradiation.

The MW power meters and temperature sensors were connected to a computer with corresponding software tools for storing and visualizing the recorded information. The MW generator was controlled by this computer as well. The leaked MWs in the air was measured by using a Leakage Detector Professional H-M2 (Appendix, Table 1, row 9), and no harmful levels (>5 mW/cm^2) were registered, even in areas close to the connectors, cables and reactors. Figure 9 illustrates this block diagram realized in hardware.

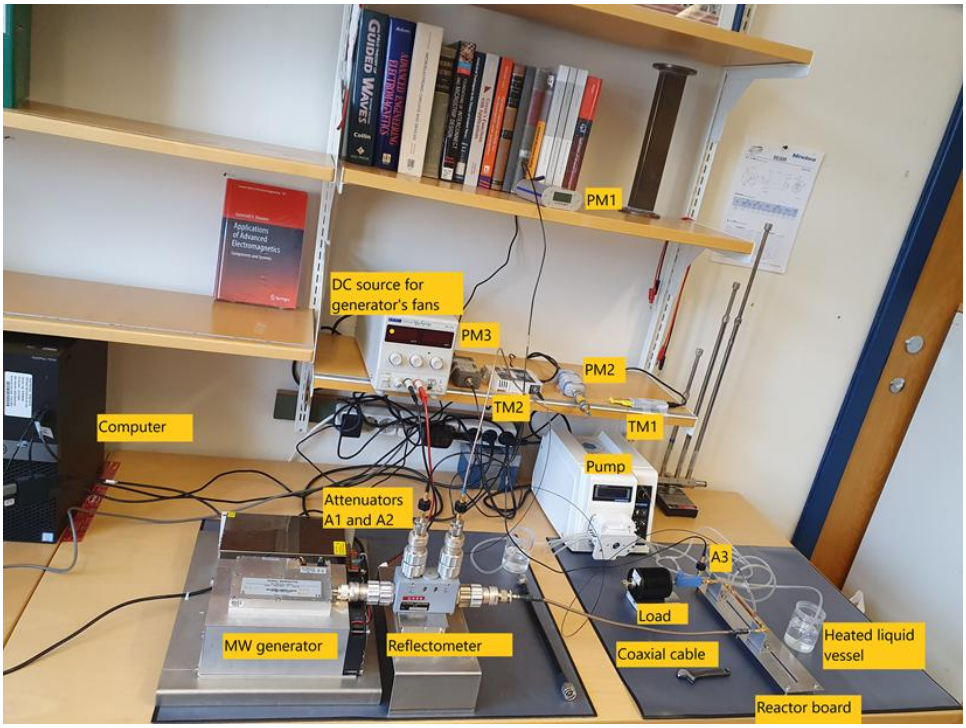

Figure 9. Measurement setup for MW-assisted liquid heating.

Because this study involved some slightly toxic and flammable liquids, all measurements were performed in our department's chemical laboratory with the help of qualified personnel. For this purpose, the setup (Figure 9) was mounted on a cart and transported to this laboratory.

5. Measurement results and discussion

5.1. Frequency characteristics of the proposed reactors

The measurements focused on the manufactured items of reactors (Figures 2–4) at a low magnitude of power and filling-liquid room temperature ($21^{\circ}C$). The first used quartz reactor sample

had a length $L = 101.5$ mm. It was filled with air (Figure 10a), ethanol (Figure 10b; see Appendix, Table 1, row 7) or acetic acid (Figure 11a; see Appendix, Table 1, row 10).

The second quartz sample had an extended length $L = 151$ mm (Figure 11b). Additionally, the examples of borosilicate glass were manufactured and measured (118 mm in size); see Figure 12.

An analysis of Figures 10b and 11 shows relatively low reflections of quartz reactors filled with ethanol or acetic acid. The inserted loss of these reactors was within the limits of 5–8 dB at 3 GHz.

For comparison, the calculated S-matrix components [44] of a regular waveguide with the same cross-sectional parameters and length loaded by 50-Ω terminations are given by red curves in Figures 10 and 11. In these calculations, the conductor loss (2) of coaxial waveguides was taken into account, and it is less in two orders than the dielectric one. Although it is a very rough model of reactors with inlets and outlets, the calculations can be used to estimate the order of the inserted loss and reflection of the studied items.

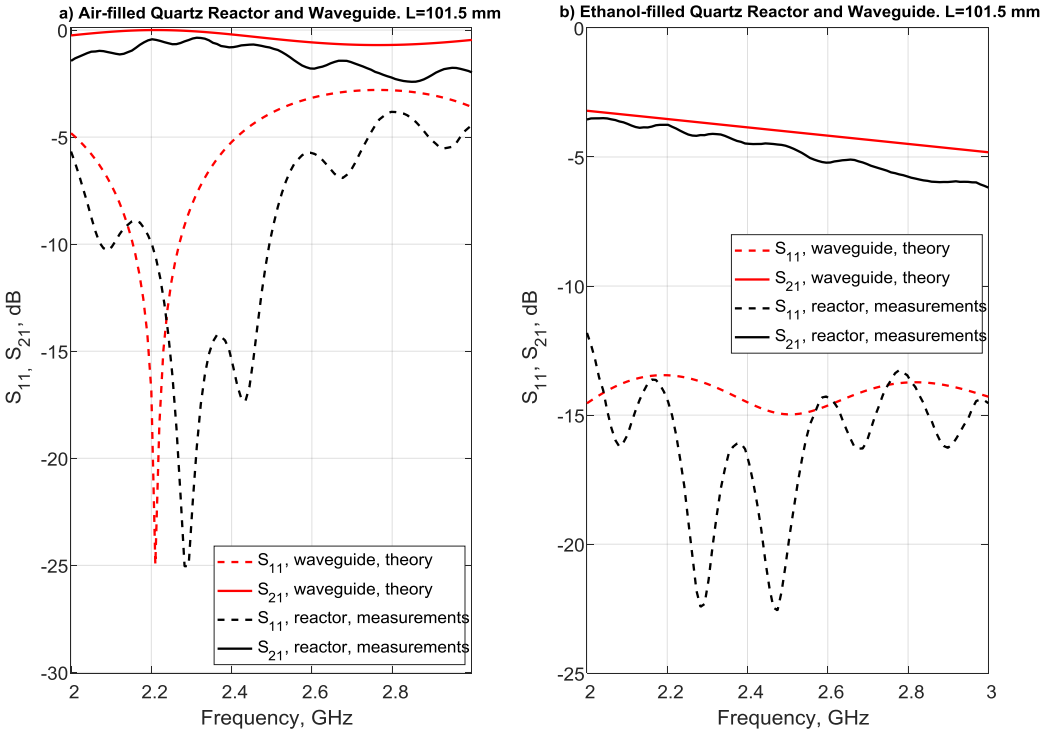

Figure 10. Measured reflection S_{11} and transmission S_{21} coefficients versus frequency for the air-filled quartz-metal reactor (a) and ethanol-filled one (b). For comparison, both plots show the analytical calculations of the same regular-length quartz-metal coaxial waveguide loaded with 50-Ω terminations in red. The measured reactor and calculated waveguide (Figure 2) length was $L = l + 2d = 101.5$ mm. The diameters of the quartz tubes were as follows: $a_0 = 0.80$ mm, $a_1 = 1.98$ mm, $a_2 = 3.89$ mm, a_3 = 5.90 mm and, for the actual silver-plated copper wire diameter, $a_C = 0.69$ mm; in the theoretical simulation, $a_C = 0.8$ mm. Other geometrical parameters of the reactor were as follows: $d = 7.73$ mm, $b = 3.91$mm and $h = 20.9$ mm, and the thickness of the inlet/outlet tubes was $t_{i/o} = 0.8$ mm.

A comparison of the short (Figure 10b) and long (Figure 11b) reactors filled with ethanol show that lengthening them increased the absorbing rate by 1–2.5 dB. The elongation decreased the excessive power that needed to be evacuated to the load L with R_L = 50 Ω. The reactors' lengthening increases the ethanol's residence time in the EM field.

Another popular solution in organic chemistry is acetic acid, i.e., CH_3CO_2H (Appendix, Table 1, row 10). It is a polar liquid, although its dielectric loss is lower than methanol and ethanol. At the industrial frequency of 2.45 GHz, its complex relative dielectric permittivity is $\varepsilon_{\text{acetic}} = 6.2 - j1.079$ [43]. For characterization, the S-matrix of a regular waveguide was calculated under the assumption that the mentioned permittivity was constant at the frequency range of 2–3 GHz. In general, it is not entirely correct. These theoretical calculations have been compared with the measurements of a reactor filled with acetic acid (Figure 11a). Again, correspondence of the S-matrices of the same length waveguide and reactor was found.

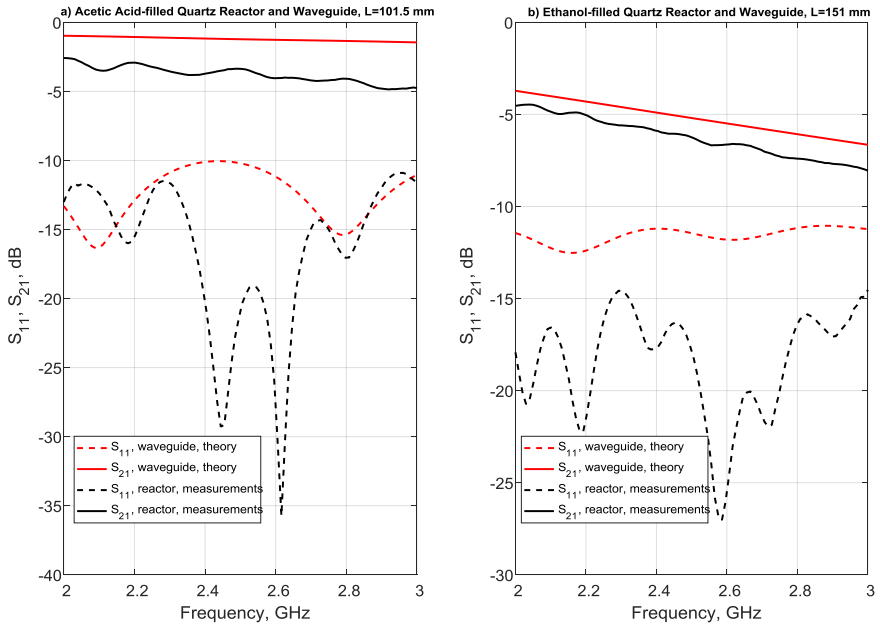

Figure 11. Measured reflection S_{11} and transmission S_{21} coefficients versus frequency for the acetic acid-filled quartz-metal reactor (a) and ethanol-filled one (b). For comparison, both plots show the analytical calculations of the same length quartz-metal coaxial waveguides loaded with 50-Ω terminations in red. The measured reactor and calculated waveguide had the following geometrical parameters: $a_0 = 0.80$ mm , $a_1 = 1.98$ mm, a_2 = 3.89 mm and $a_3 = 5.90$ mm. The actual silver-plated copper wire diameter was $a_C = 0.69$ mm; in the theoretical simulation, $a_C = 0.8$ mm. Other geometrical parameters of the reactors were as follows: $d = 7.73$ mm, $b = 3.91$mm and $h = 20.9$ mm , and the thickness of the inlet/outlet tubes was $t_{i/o} = 0.8$ mm . The acetic acid-filled reactor (a) had a length $L = l + 2d = 101.5$ mm . The ethanol-filled reactor length was $L = 151$ mm.

It can be seen in Figure 11a that the reflection coefficient S_{11} of the acid-filled reactor was relatively low, so the inserted loss was strongly coupled to liquid absorption; it was around 3.47 dB at 2.45 GHz.

Another glass material used in chemistry is borosilicate, which has silica and boron trioxide as the main glass-forming constituents; the experimental results are shown in Figure 12. The permittivity of this glass depends on the chemical contents and varies in the range of $\varepsilon' = 4.1 - 6.7$ [39]. The polarization loss tangent was on the order of 10^{-3}. Several reactors were manufactured by using this material (Appendix 1, Table 1, row 1). Unfortunately, accurate data on the dielectric properties are not known by the manufacturer. The study of reactors of this type has only been experimental.

Figure 12a shows the measurement results for a borosilicate reactor filled with air, methanol or ethanol. It can be seen that the air-filled reactor had increased reflection, and it was unmatched to 50 Ω. Filling this reactor with methanol and ethanol was found to drive the reflection coefficient S_{11} below -10 dB, which is still good enough for the devices without matching. Ethanol showed better absorption due to its higher loss as compared to methanol.

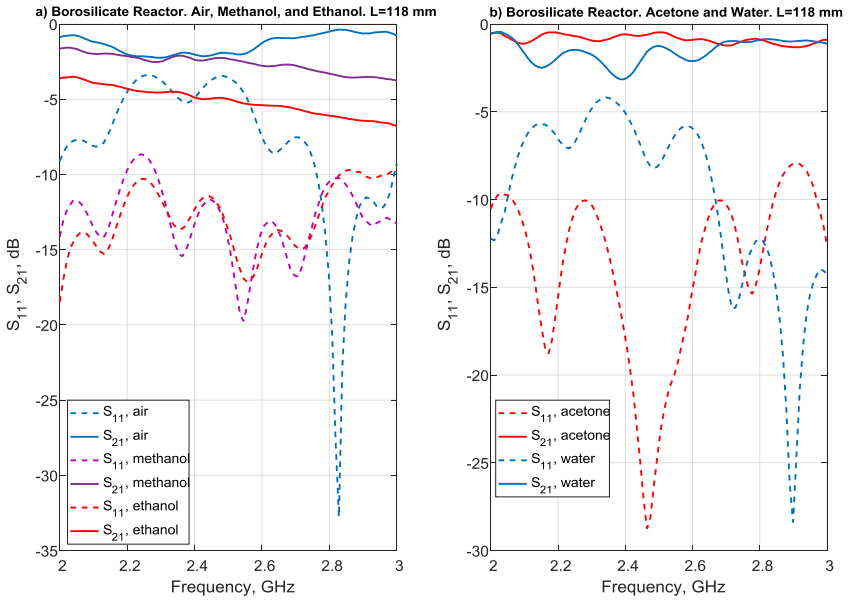

Figure 12. Measured reflection S_{11} and transmission S_{21} coefficients versus frequency for borosilicate glass reactors. (a) Reactors filled with air, methanol or ethanol. (b) Reactors filled with acetone or reverse osmosis water (Appendix, Table 1, row 13). The diameters of the borosilicate tubes were as follows: $a_0 = 0.59$ mm , $a_1 = 1.94$ mm, $a_2 = 3.91$ mm, a_3 = 5.88 mm and, for the silver-plated copper wire diameter, $a_C = 0.48$ mm. The reactor's length was $L = l + 2d = 118$ mm ; additionally, $d = 7$ mm , $b = 3.91$mm , $h = 20.5$ mm and the thickness of the inlet/outlet tubes was $t_{i/o} = 0.72$ mm .

Additional results (Figure 12b) have been obtained for a borosilicate reactor filled with acetone, i.e., $(CH_3)_2 CO$ (Appendix, Table 1, row 12), or reverse osmosis water (Appendix, Table 1, row 13). These liquids are less lossy than spirits. For instance, acetone at 2.45 GHz has a permittivity of $\varepsilon'_{ace} = 20.7$ and $\tan\delta_{ace} = 0.054$ [43], i.e., a small loss. Anyway, this reactor shows a low reflection, i.e., below -20 dB.

Water has a very high real part of permittivity ε' and relatively low dipolar loss [13,43]. It leads to a significant mismatch of our reactors filled with water (Figure 12b). Besides, the dielectric parameters of water are highly dependent on temperature and frequency [13], which makes this liquid more challenging to heat. Then, unfortunately, our reactors intended for heating liquids of lower permittivity should be re-designed for water.

The results of characterization in the frequency domain show that, for liquids with a relative permittivity range of $\varepsilon' = 3.75 - 30$, the reactors with the current geometry that were made of fused quartz and borosilicate glass were matched well to the 50-Ω environment. These conclusions are confirmed by the heating experiments, which are considered below.

5.2. MW heating of reference liquids in the developed glass-metal reactors

The thermal characterization of reactors was performed by using the above-considered measurement test fixture and setup (Figures 4, 8 and 9). The liquid temperature was measured every 0.5 s by using an OSENSA fiber optic thermometer (Appendix, Table 1, row 22), whose resolution is $0.01\,^{\circ}\mathrm{C}$. The sensor of this instrument was installed precisely at the reactor opening of the outlet's glass tube in each case. After each measurement period, the reactor was cooled down by using a room-temperature liquid and air from a nearby standing fan. The following two pumping rates were applied: 3 and 6 mL/min. The generator's power was changed from 10 to 40 W in most cases, except in the experiments with water heating.

Although our reactors have not been designed for high-permittivity and low-loss liquids like water ($\varepsilon'_{\text{water}} = 78.74$ and loss tangent $\tan\delta_{\text{water}} = 0.134$ [13]), the heating process for this liquid was studied despite there being a high reflection coefficient from these reactors (see Figure 12b). The plot below (Figure 13) shows the results of heating this relatively low-loss liquid in a borosilicate reactor.

It is seen that a strong reflection (Figure 12b) and relatively low loss led to poor heating, requiring increased power consumption of water-filled samples (Figure 13). Strong reflection can be avoided by applying better external matching, re-designing reactors, using water mixtures with alcohols to increase the EM absorption [45], etc.

The picture changed radically when pure alcohol was heated. Some typical results of thermal characterization are shown below for a quartz reactor (Figure 14). Two liquid rate flows were applied: 3 and 6 mL/min. The generator power was increased step wisely from 20 to 40 W. Possible EM power leakage was controlled by every power switch through the use of the MW indicator mentioned above.

Figure 14a shows the results of heating ethanol at a pump flow rate of 3 mL/min. In fact, 30 W of MW power was enough to reach the ethanol's boiling point ($78.37\,^{\circ}\mathrm{C}$).

Meanwhile, there were some temperature picks found over the boiling temperature temperatures of ethanol (Figure 14). It means that the MW overheating effect (known from many published experiments) occurred in this degassed liquid. Unfortunately, this overheating effect is unstable at low liquid pressure, and the temperature fluctuated up and down under the conditions of both pumping regimes, 3 mL/min (Figure 14a) and 6 mL/min (Figure 14b). The measurements were repeated with ethanol enriched by air and vapor, and no overheating occurred then.

In the case of methanol, which is less lossy than ethyl alcohol, overheating occurred only with the 3-mL/min regime and applied power of 40 W (Figure 15a). A higher pump flow rate did not show this effect, but the curve distortions indicate some bubbling in the vessel, except for the 20-W curve (Figure 15b).

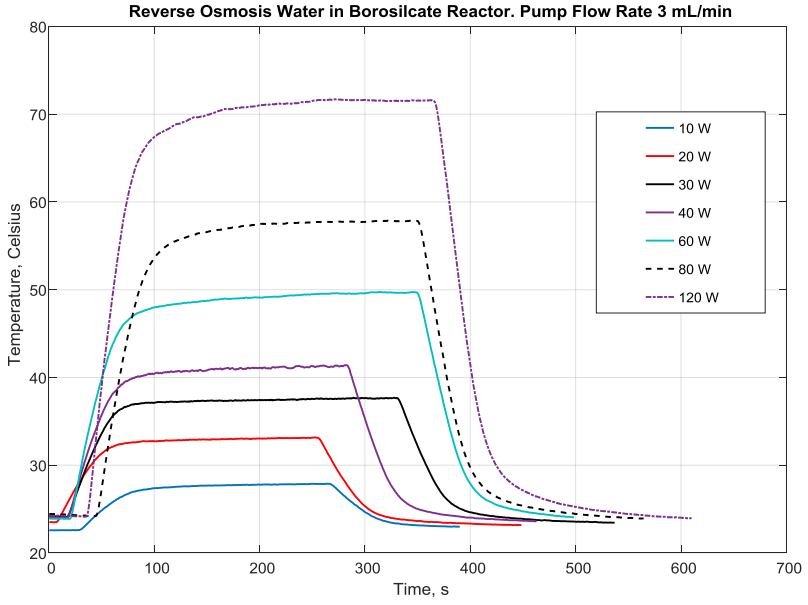

Figure 13. Temperature trends at the borosilicate reactor's outlet for reverse osmosis water at a pump flow rate of $3\ \mathrm{mL/min}$. The reactor's length was $L = l + 2d = 118$ mm, $d = 7$ mm, $b = 3.91$mm, $h = 20.5$ mm and the thickness of the inlet/outlet tubes was $t_{i/o} = 0.72$ mm. The diameters of borosilicate tubes were as follows: $a_0 = 0.59$ mm, $a_1 = 1.94$ mm, $a_2 = 3.91$ mm, a_3 = 5.88 mm and, for the actual silver-plated copper wire diameter, $a_C = 0.48$ mm.

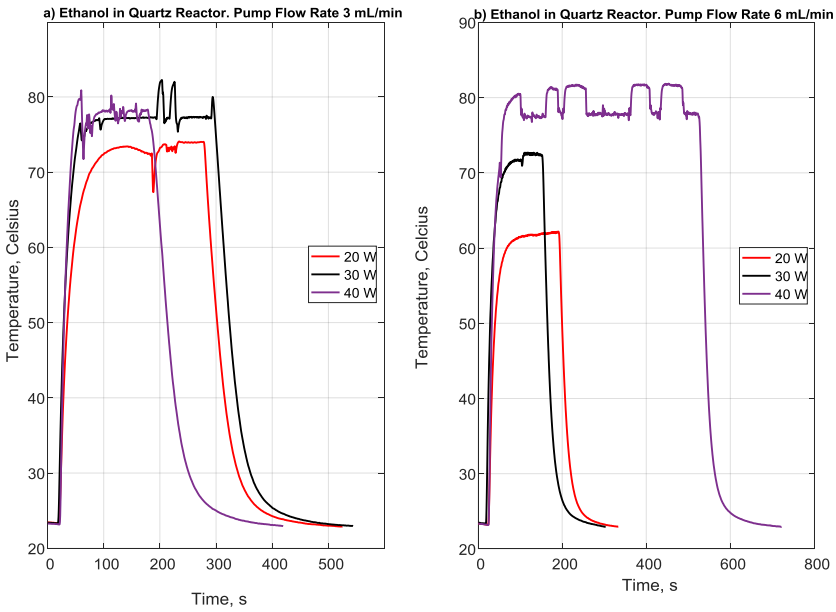

Figure 14. Temperature trends at the quartz reactor's outlet for ethanol at pump flow rates of $3\ \mathrm{mL/min}$ (a) and $6\ \mathrm{mL/min}$ (b). The reactor (Figure 2) length was $L = l + 2d = 101.5$ mm, $d = 7.73$ mm, $b = 3.91$mm and $h = 20.9$ mm. The diameters of the quartz tubes (see Figures 2 and 5) were as follows: $a_0 = 0.80$ mm, $a_1 = 1.98$ mm, $a_2 = 3.89$ mm, a_3 = 5.90 mm and, for the actual silver-plated copper wire diameter, $a_C = 0.69$ mm; the thickness of the inlet/outlet tubes was $t_{i/o} = 0.8$ mm.

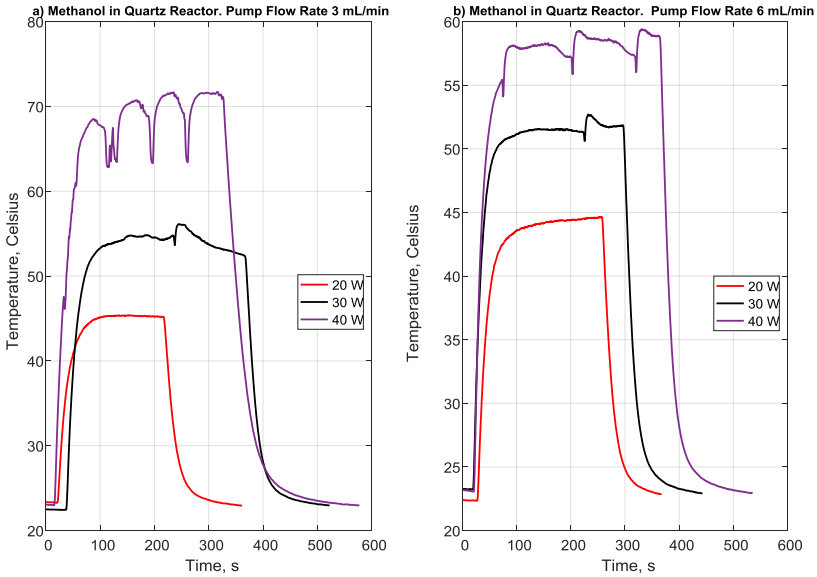

Figure 15. Temperature trends at the quartz reactor's outlet for methanol with pump flow rates of 3 mL/min (a) and 6 mL/min (b). The reactor (Figure 2) length was $L = l + 2d = 101.5$ mm, $d = 7.73$ mm, $b = 3.91$mm and $h = 20.9$ mm. The diameters of quartz tubes were $a_0 = 0.80$ mm, $a_1 = 1.98$ mm, $a_2 = 3.89$ mm, $a_3 = 5.90$ mm and, for the actual silver-plated copper wire diameter, $a_C = 0.69$ mm; the thickness of the inlet/outlet tubes was $t_{i/o} = 0.8$ mm.

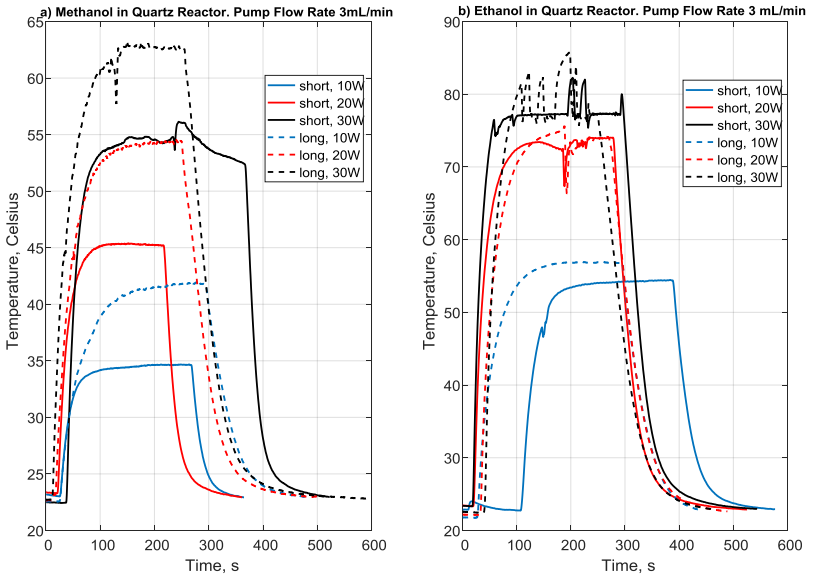

Figure 16. Temperature trends at the quartz reactor's outlets for methanol (a) and ethanol (b) at a pump flow rate of 3 mL/min, and given for short $(L = 101.5$ mm$)$ and long $(L = 151.5$ mm$)$ reactors at different applied powers. Reactor geometry: $d = 7.73$ mm, $b = 3.91$mm and $h = 20.9$ mm. The diameters of the quartz tubes were $a_0 = 0.80$ mm, $a_1 = 1.98$ mm, , $a_2 = 3.89$ mm, $a_3 = 5.90$ mm and, for the actual silver-plated copper wire diameter, $a_C = 0.69$ mm; the thickness of the inlet/outlet tubes was $t_{i/o} = 0.8$ mm.

The quartz reactors with an increased length $\left(L = l + 2d = 151\ \text{mm}\right)$ were manufactured with the idea that these reactors allow for a longer residence time of liquids in the axis-extended MW field and that they will provide higher temperatures. It was confirmed with heating methanol (Figure 16a) when this longer reactor provided higher temperatures in the saturation regimes for 10–30 W of the applied MW power.

The ethanol-filled reactor (Figure 16b) had a higher loss than the methanol-filled one (Figure 16). Even 20 or 30 W of power was able to drive ethanol close to its boiling point $78.37\ ^{\circ}\text{C}$, where the temperature of the liquid coming to the intense heating area and the reactor's outlet does not play a significant role. Besides, ethanol caused a shorter modal penetration depth in our reactors, and the moving liquid had a reduced residence time in a strong heating MW field as compared to the methanol-filled reactors. It makes the saturation regime less sensitive to the reactor length. It is supposed that the mentioned difference would be brighter for slower-moving ethanol.

6. Conclusions

In this paper, a novel glass-metal coaxial reactor has been proposed for MW-assisted liquid heating. Compared to known hollow coaxial designs, it was composed of two concentric glass tubes. One is for the central conductor carrying MW current, and the other copper-foiled pipe surrounding the first tube was for the narrow cavity of a cylindrical shape filled with a lossy liquid heated by the current's EM field. The thin shielded glass tubes, melted orthogonally to the reactor's body and opened into this cylindrical cavity, were to provide the liquid flow.

These reactors, consisting of three-layer coaxial waveguides, have been designed to be relatively insensitive to the cavity-filled liquids, whose relative permittivity was in the range of $\varepsilon = 3.75 - 30$ at frequencies of 1–3 GHz and temperatures up to the fluids' boiling points.

Several reactors made of quartz and borosilicate glass were designed and characterized by using analytical, numerical and experimental methods in the frequency, temperature and time domains for methanol, ethanol, acetone, acetic acid, ethylene glycol and 1,2-propanol. The heating of methanol, ethanol and water flow has been studied by using a developed setup consisting of a high-power adjustable MW 250-W generator, power- and temperature-controlling instrumentation and liquid-handling hardware units. The applied power needed to boil ethanol and methanol was around 20–40 W. lengthening the reactors led to higher output temperatures in the saturation regimes and longer residence times of the liquids in the strong heating field. The effect of MW overheating on the studied fluids in flow regimes has been discovered.

These developed reactors, as manufactured by using low-cost technology, are usable in the 50-Ω environment. They have shown their stability towards the variations of the dielectric permittivity of heated liquids. The design prevents corrosion of conductors in aggressive fluids and excludes the electric discharging effect in conducting liquids. The narrow reactor's fluid-filled channels diminish the radial convection of homogeneously MW-heated liquids, and it can increase the predictability of the yield of chemical reactions.

Acknowledgments

The authors thank the IE Faculty Fund (NTNU) for Small-Scale Projects and the Department of Electronic Systems (NTNU) for financial and technical support. The help of S. Pettersen, the Head of the Chemistry Laboratory in this department, is appreciated for his consultation and assistance.

Conflict of interest

The authors declare that there is no conflict of interest.

References

1. Loupy A (2006) *Microwaves in Organic Synthesis*. Weinheim: Wiley-VCH. https://doi.org/10.1002/9783527619559
2. Kappe C, Stadler A, Dallinger D (2012) *Microwaves in Organic and Medicinal Chemistry*. Weinheim: Wiley-VCH. https://doi.org/10.1002/3527606556
3. Metaxas A, Meredith R (2008) *Industrial Microwave Heating*. Milton Keynes, UK: Lightning Source UK Ltd.
4. Li M, Wu X, Han D, et al. (2022) A high-efficiency single-mode traveling wave reactor for continuous flow processing. *Processes* 10: 1261. https://doi.org/10.3390/pr10071261
5. Nikawa Y (2016) Measurement of temperature dependent permittivity of liquid under microwave heating. *Proc 2016 IEEE MTT-S Int Microw Symp* (IMS), 1–4. https://doi.org/10.1109/MWSYM.2016.7540089
6. Miyakawa M, Kanamori S, Hagihara K, et al. (2021) Cylindrical resonator-type microwave heating reactor with real-time monitoring function of dielectric property applied to drying processes. *Ind Eng Chem Res* 60: 9119–9127. https://doi.org/10.1021/acs.iecr.1c00569
7. Topcam H, Karatas O, Erol B, et al. (2020) Effect of rotation on temperature uniformity of microwave processed low-high viscosity liquids: A computational study with experimental validation. *Innov Food Sci Emerg* 60: 102306. https://doi.org/10.1016/j.ifset.2020.102306
8. Navarro M (2020) Water, toluene, and ethanol under microwave irradiation: numerical simulations of the effect of the vessel's size. *J Heat Transfer* 142: 102104. https://doi.org/10.1115/1.4047512
9. Son E, Coskun E, Ozturk S, et al. (2022) Microwave decontamination process for hummus: A computational study with experimental validation. *Innov Food Sci Emerg* 82: 103162. https://doi.org/10.1016/j.ifset.2022.103162
10. Khaghanikavkani E, Farid M, Holdem J, et al. (2013) Microwave pyrolysis of plastic. *J Chem Eng Process Techn* 4: 1000150. https://doi.org/10.4172/2157-7048.1000150
11. Mitani T, Hasegawa N, Nakajima R, et al. (2016) Development of a wideband microwave reactor with a coaxial cable. *Chem Eng J* 299: 209–216. http://dx.doi.org/10.1016/j.cej.2016.04.064
12. Kapranov S and Kouzaev G (2015) Scalable reactor for microwave-and ultrasound-assisted chemistry. GB Patent Appl. GB1504690.7A dated on 2015-03-19. *IPO Patent Searchable Patents J* 6572: dated 06.05.2015. Available from: https://patents.google.com/patent/GB2536485A/en?inventor=Kouzaev+Guennadi
13. Kapranov S, Kouzaev G (2017) Models of water, methanol, and ethanol and their applications in the design of miniature microwave heating reactors. *Int J Thermal Sci* 122: 53–73. https://doi.org/10.1016/j.ijthermalsci.2017.08.007
14. Kouzaev G (2017) A method and apparatus for separate supply of microwave and mechanical energies to liquid reagents in coaxial rotating chemical reactors. GB Patent Appl. GB1704095.7 dated 15 March 2017. *IPO Patent Searchable Patents J 6675* dated 26.04.2017. Available from: https://patents.google.com/patent/GB2560545A/en

15. Kapranov S, Kouzaev G (2019) Study of microwave heating of reference liquids in a coaxial waveguide reactor using the experimental, semi-analytical, and numerical means. *Int J Thermal Sci* 140: 505–520. https://doi.org/10.1016/j.ijthermalsci.2019.03.023
16. Kouzaev G, Kapranov S (2020) Microwave miniature coaxial reactors for on-demand material synthesis. *TechRxiv Preprint*. https://doi.org/10.36227/techrxiv.11649678.v2
17. Sarabi F, Chorbani M, Stankiewicz A, et al. (2020) Coaxial traveling-wave microwave reactors: Design challenges and solutions. *Chem Eng Res Design* 153: 677–683. https://doi.org/10.1016/j.cherd.2019.11.022
18. Kouzaev G (2022) Glass-metal coaxial-waveguide reactors for on-demand microwave-assisted chemistry. *TechRxiv Preprint.* https://doi.org/10.36227/techrxiv.20045006.v2
19. Shi WD, Wang C, and Yan WC (2022) Model-based design and operation of coaxial-probe-type microwave reactor toward large-scale production of nanoparticles. *Chem Eng Sci* 264: 118162. https://doi.org/10.1016/j.ces.2022.118162
20. Shah J, Sundaresan S, Geist J, et al. (2007) Microwave dielectric heating of fluids in an integrated microfluidic device. *J Micromech Microeng* 17: 2224–2230. https://doi.org/10.5772/53881
21. Issadore D, Humphry K, Brown K, et al. (2009) Microwave dielectric heating of drops in microfluidic devices. *Lab Chip* 9: 1701–1706. https://doi.org/10.1039/b822357b
22. Khayari A, Medrano M, Verlagio E, et al. (2011) Microwave-induced water flow in a microchannel built on a coplanar waveguide. *J Appl Phys* 110: 064912. https://doi.org/10.1063/1.3641516
23. Koziej D, Floryan C, Spering R, et al. (2013) Microwave dielectric heating of non-aqueous droplets in a microfluidic device for nanoparticle synthesis. *Nanoscale* 5: 5468–5475. https://doi.org/10.1039/C3NR00500C
24. Mascia S, Heider P, Zhang H (2013) End-to-end continuous manufacturing of pharmaceuticals: integrated synthesis, purification, and final dosage formation. *Angew Chem Int Ed* 52: 12359–12363. https://doi.org/10.1002/anie.201305429
25. Li J, Ballmer S, Gillis E, et al. (2015) Synthesis of many different types of small organic molecules using one automated process. *Science* 347: 1221–1226. http://dx.doi.org/10.1126/science.aaa5414
26. Kitson P, Marie G, Francoia J, et al. (2018) Digitization of multistep organic synthesis in reactionware for on-demand pharmaceuticals. *Science* 359: 314–319. https://doi.org/10.1126/science.aao3466
27. Shibata K, Kobayashi M (2015) Measurement of complex permittivity for liquids using the coaxial line reflection method. *Proc APEEMC'2015*, 452–455. https://doi.org/10.1109/APEMC.2015.7175237
28. Jensen W (2006) The origin of the Liebig condenser. *J Chem Educ* 83: 23. https://doi.org/10.1021/ed083p23
29. RG401 Coax Cable. *Technical Data Sheet*. 2022. Available from: https://www.pasternack.com/images/ProductPDF/RG401-U-FT.pdf
30. Ott H (2009) *Electromagnetic Compatibility Engineering*. NY: J. Wiley & Sons.
31. Shielding Effectiveness of Expanded Metal Foils (EMFs). Dexmet Corp. 2022. Available from: https://cdn2.hubspot.net/hubfs/3798930/assets/PDF%20files/Shielding_Effectiveness_82017.pdf

32. Kouzaev G (2013) *Applications of Advanced Electromagnetics. Components and Systems*. Berlin Heidelberg: Springer Verlag.
33. Mcintosh R, Turgeon L (1973) Propagation along transversely inhomogeneous coaxial transmission lines. *IEEE T Microw Theory* 21: 139–142. https://doi.org/10.1109/TMTT.1973.1127949
34. Mitelman Y (2019) A novel method for inhomogeneous coaxial line analysis. *Proc 2019 Ural Symp Biomedical Eng., Radioelectronics and Inform Technology (USBERIT)*, 458–461. https://doi.org/10.1109/USBEREIT.2019.8736605
35. Wand W, Al-Charchafchi S (1998) Using equivalent dielectric constant to simplify the analysis of patch microstrip antenna with multi layer substrate. *IEEE Antenn Propag Soc Int Symp, Digest* 2: 676–679. https://doi.org/10.1109/APS.1998.702028
36. Nikol'skii V and Nikol'skaia T (1989) Electrodynamics and Radiowave Propagation. Moscow: Nauka Publ. (in Russian).
37. Gunston M (1972) *Microwave Transmission-Line Impedance Data*. NY: Van Nostrand Reinhold Comp. Ltd.
38. Comsol Multiphysics. Available from https://www.comsol.com
39. Komarov V (2012) *Handbook of Dielectric and Thermal Properties of Materials at Microwave Frequencies*. Artech House.
40. Michalski K, Mustafa M (2018) On the computation of hybrid modes in planar layered waveguides anisotropic conductive sheets with multiple anisotropic conductive sheets. *Proc R Soc A* 474: 20180288. http://dx.doi.org/10.1098/rspa.2018.0288
41. Tyszkiewicz C (2012) Sensing properties of four-layered planar waveguide design. Theoretical analyses. *Acta Polonica A* 122: 908–914. https://doi.org/10.12693/APhysPolA.122.908
42. Sengwa R, Kaur K, Chaudhary R (2000) Dielectric properties of low molecular weight poly(ethylene glycol)s. *Polymer Int* 49: 599–608.
43. Dielectric properties of solvents. 2022. Available from: https://cem.com/cn/microwave-chemistry/solvent-choice
44. Gupta K, Garg R, Chadha R (1981) *Computer-aided Design of Microwave Circuits*. Artech House.
45. Bao JZ (1996) Microwave dielectric characterization of binary mixtures of water, methanol, and ethanol. *J Chem Phys* 104: 4441. https://doi.org/10.1063/1.471197

Appendix

Table 1. Commercially available parts, instruments and materials used in experiments and their main characteristics.

Item Number	Notations in the Text	Part Name	Manufacturer	Parameters
1	Condenser	Miniature Liebig Borosilicate Condenser	*Andrews Glass Co.*	$L = 118$ mm
2	Condenser	Miniature Liebig Quartz Condenser	*Sandfire Scientific, Ltd.*	$L = 101$ mm
3	Condenser	Miniature Liebig Quartz Condenser	*Sandfire Scientific, Ltd.*	$L = 151$ mm
4	Copper foil	Copper Foil	*Lpraer/Amazon*	Thickness: 0.05 mm One-side acryl-based conductive adhesive layer

5	SMA connector	Coaxial Connectors SMA ST Plug Solder .250 Semi-Rigid	*RF Amphenol*	Gold-plated
6	Solder paste	Solder Paste ChipQuick SMDLTLFP	*ChipQuik, Inc.*	87% metal by weight
7	C_2H_5OH	Ethanol	*Kiilto*	98% purity
8		Network Analyzer NanoVNA V2 Plus4 Pro	*HCXQS group*	Bandwidth: 50 kHz–4 GHz
9		Microwave Leakage Detector Professional H-M2	*Amazon*	Frequency: 2.450 GHz
10	CH_3CO_2H	Acetic acid	*Sigma Aldrich*	99% purity
11	CH_3OH	Methanol	*VWR*	95% purity
12	$(CH_3)_2CO$	Acetone	*VWR*	98% purity
13	H_2O	Reverse Osmosis Water	*RIOS 50 Merckmillipore*	Water resistivity: 18 MΩ-cm
14	MW Generator	KU SG 2.45-250A - Signal Generator	*Kuhne Electronics. Microwave Components*	Frequency: 2.45 GHz Output power: 0–250 W
15	Reflectometer	ZDP-BN 35691	*Rohde&Schwartz*	Frequency range: 300 MHz–4.2 GHz
16	PM_1	Power Meter MA24126A	*Anritsu*	Frequency range: 10 MHz–26 GHz
17	PM_2	Power Meter KU PM BB 001800 A	*Kuhne electronics. Microwave Components*	Frequency range: 10 MHz–8 GHz
18	L	Termination SAT8S-100F	*Fairview Microwave*	Maximal Power: 100 W
19	DC	Directional Coupler SC3022116	*SigaTeK*	Coupling: 20 dB
20	PM_3	Power Meter NRP-Z22	*Rohde&Schwartz*	Frequency range: 10 MHz–18 GHz
21	A_1	Attenuator MCL	*Microcircuits*	Inserted loss: 10 dB
22	A_2	Attenuator MCL	*Microcircuits*	Inserted loss: 10 dB
23	A_3	Attenuator MCL	*Microcircuits*	Inserted loss: 20 dB
24	Coaxial cable	Interconnect Coaxial Cables Sucoflex 104P	*Huber+Suhner*	Attenuation: <1.5 dB m^{-1}
25	TM_2	Thermocouple Meter UTC USB K with Probe KMTSS-IM025G-150	*Omega Engineering*	Max temperature measurement error: 1° C
26	Pump	Peristaltic Dispensing Pump LP-BT100-1F/DG-4(10)	*Drifton*	Speed: 0.1–100 rpm. Flow rate: 0.2 µL/min to 500 mL/min
27	TM_1	Fiber Optic Temperature Transmitter FTX-100-LUX+ and Fiber Optic Sensor PRB-G-40	*Osensa Innovations*	Temperature resolution: 0.01 ° C